iSTEAM Communications ISSN:2691-7300 www.iSTEAMC.com

Research Article in Physics

Surface Gravity Wave Generation and Interference Effects in SPH Models

Zijun Shen[1,*]

[1] Kang Chiao International School Xi'an Campus, Xi'an, Shaanxi , China

[*] Correspondence: jasonshen0518@gmail.com

(Received: 10/31/2022; Accepted: 12/27/2022; Published: 12/30/2022)

DOI: https://doi.org/10.37906/isteamc.2022.8

Abstract: DualSPHysics is an open-source implementation of the SPH (smoothed-particle hydrodynamics) particle mechanics model built for applications in coastal and ocean engineering, suitable for cases possessing complex surface boundary conditions and interactions of fluids with bound objects. This work seeks to examine the general plausibility of utilization of DualSPHysics for modeling cases involving the diffraction and interference effects of surface gravity waves. The work attempts to seek optimized parameters for wave generation intended to be used in diffraction and interference cases at lower simulation resolutions by taking advantage of simulation parameters such as gravity, construct simple examples to demonstrate the plausibility to use the model with more complex cases (possibly involving diffraction and interference off lattices), and validate wave behaviors (related to gravity) within the model using accepted theories of surface wave propagation. The paper identifies several limitations whose mitigation was deemed necessary for further success applying DualSPHysics to diffraction and interference problems, as well as further analysis and tests needed for a complete assessment of the tested cases.

Keywords: CFD, Meshless, Smoothed-particle hydrodynamics, Diffraction, Interference, Surface gravity waves.

1. Introduction

Smoothed-particle hydrodynamics, or SPH, is a computational method used for the simulation of particle mechanics. SPH, a meshless method where nodes (particles) are not interconnected, is highly suitable for modeling free-surface flow, where models flexible enough to accommodate for complex boundary conditions are favored (Violeau & Rogers, 2016). Such properties make it ideal for applications in coastal engineering, such as in recent examples Draycott *et al*. (2022) and Lowe *et al*. (2022)

SPHysics is an SPH computational fluid dynamics model for weakly-compressible flow with focus on simulating violent coastal/offshore phenomena and their effects on coastal/offshore infrastructure (Domínguez, et al., 2021). DualSPHysics is an open-source project developed to address computational expense of the SPHysics model involving high particle counts by making use of the Graphical Processing Unit. In addition to the SPH Solver, the current DualSPHysics release includes dedicated pre- and post-processing tools (Domínguez, et al., 2021). As the model is obviously designed with the intention of use in coastal engineering and ocean modeling, this paper seeks to examine the plausibility of using DualSPHysics to accurately portray less-than-obviously-intended scenarios, namely, to examine the diffraction and interference of regular surface gravity waves, whose generation although well-characterized by Hughes (1993), lacks satisfactory insight into more complex wave behavior in the SPHysics model. Using cases such as the double-slit interference, we examine wave behavior in well-

known examples familiar to quantum mechanics and classical electromagnetism. These simple cases are meant to give us insight into the propagation of surface waves through complex lattice structures within SPHysics. Furthermore, a point was made to limit the applied tools and methods to those included in the DualSPHysics code up to data collection.

2. Research Design, Data collection and analysis Methods

2.1. Wave Optimization

It is essential, at first, to investigate how surface gravity waves are generated and behave in the SPHysics model and to identify the best parameter values to be used for the purpose at hand.

DualSPHysics provides well-understood methods for generating one-dimensional surface wave, designed to be used for moving boundaries (flaps/pistons). These are fine-tuned by a set of inputs related to the properties of the target wave: the displacement X_0 of these wavemakers is given by (Domínguez, et al., 2021).

$$X_0(t) = \frac{H}{2m_{cr}} sin(wt + \phi) + \left[\left(\frac{H^2}{32\left(1 - \frac{d}{2(d + d_0)}\right)}\right)\left(\frac{3cosh(kd)}{sinh^3(kd)} - \frac{2}{m_{cr}}\right)\right] sin(2wt + 2\phi), \tag{1}$$

in which m_{cr} is given by

$$m_{cr} = \frac{4sinh(kd)}{sinh(2kd) + kd}\left[sinh(kd) + \frac{1 - cosh(kd)}{k(d + d_0)}\right], \tag{2}$$

such that the input parameters are met, where H is the wave height, ω is the angular frequency, k is the wavenumber, d is the initial water depth, ϕ is the initial phase, and d_0 is a parameter related to the location of the hinge for flap wavemakers ($d_0 = \infty$ for pistons). For more detail about Equations 1 and 2, see Dominguez et al. (2021) and DualSPHysics documentations. Figure 1 shows a two-dimensional piston - a simple example of a moving boundary wavemaker. Such a wavemaker is excellent for producing surface gravity waves for two-dimensional simulations or three-dimensional simulations where wave action is inherently two-dimensional. The piston moving boundary wavemakers would prove to be immensely useful for the early stages of research, where two-dimensional simulations are more efficient and easier to work with.

For the purpose of examining interference and diffraction, on the other hand, we are more concerned with simulating waves at the full three dimensions. More specifically, we would like to produce radially propagating regular surface waves from point-like wavemakers. One suitable apparatus is a vertically oscillating downwards-pointed cone, such as shown in Figure 2. Its motion along z-axis is governed by a simple sinusoidal function:

$$Z_0(t) = Re^{iwt+\phi}, \tag{3}$$

where z_0 is the z-displacement, R is the amplitude, ω is the angular frequency, and ϕ is the initial phase. Unlike Equation 1, these parameters are not related to the generated waves but the wavemaker itself. This was the apparatus selected for point wave source generation throughout the paper.

2.1.1. Investigation of Gravity as a Parameter to Extend Wave Lifetime

One of the elusive obstacles of generating waves within the SPHysics model with intention of observing diffraction and interference is the limited lifetime of the surface waves. Typically, SPHysics wavemaker example cases use wavemakers with stroke-lengths comparable to the scale of the simulation domain, therefore waves are easily detectable at the edges of the domain. Such a practice applied to a point wave source, such as a cone, does not yield satisfactory results. In an attempt to extend the longevity of the waves, one may decide to change the various operation parameters of the simulation. This section is dedicated to the investigation of the effects of varying gravity on the longevity and other quantifiable properties of generated waves as a possible parameter to extend wave lifetime.

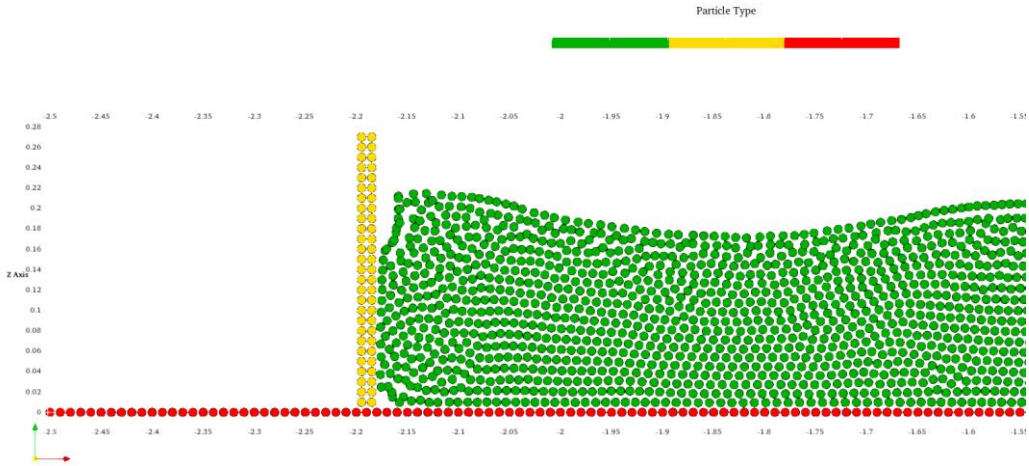

Figure 1. Preset wave generation: piston (yellow) moving along the x-axis according to equation 1 and equation 2.

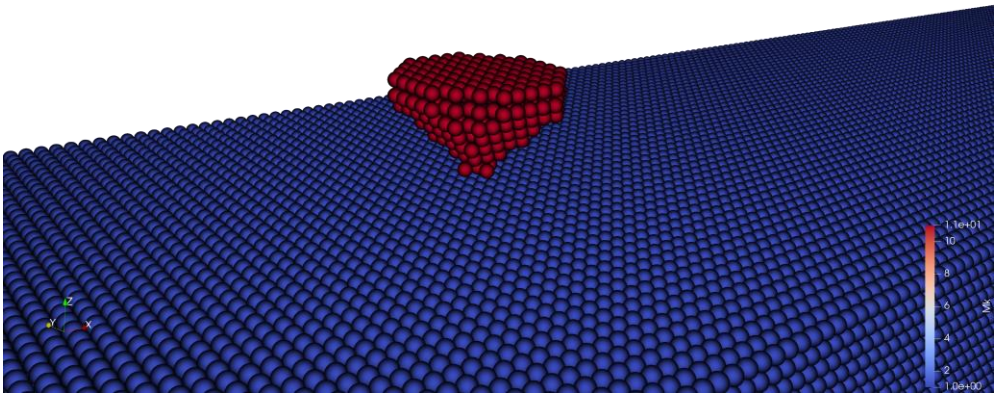

Figure 2. Cone-shaped wave generator (red), fluid (blue). Visualized in *Paraview*.

For now, let us ignore the need of a point wave source. The correlation between g and the longevity of piston (Figure 1) generated wave for g = 10 to 20 and a larger range of $10 \cdot 2^{-1}$ to $10 \cdot 10^{4}$ is shown in Figure 3 (a) and (b), respectively. From these plots, even though the data is limited in both scale and resolution, a reasonably clear relationship between gravity and the wave lifetime can be established, at

least for g values within our working range. Note that at higher gravity levels of g = 160 for the piston wavemaker, the size of generated waves become comparable to the length of the domain, so that only one wave may be present at any given time.

It is also possible to see from Figure 3 that, for the piston wavemaker, an increase in g corresponds to an increase in the initial amplitude of generated waves. Although further trials have shown that the same relationship does not hold valid for other flavors of wave generator designs.

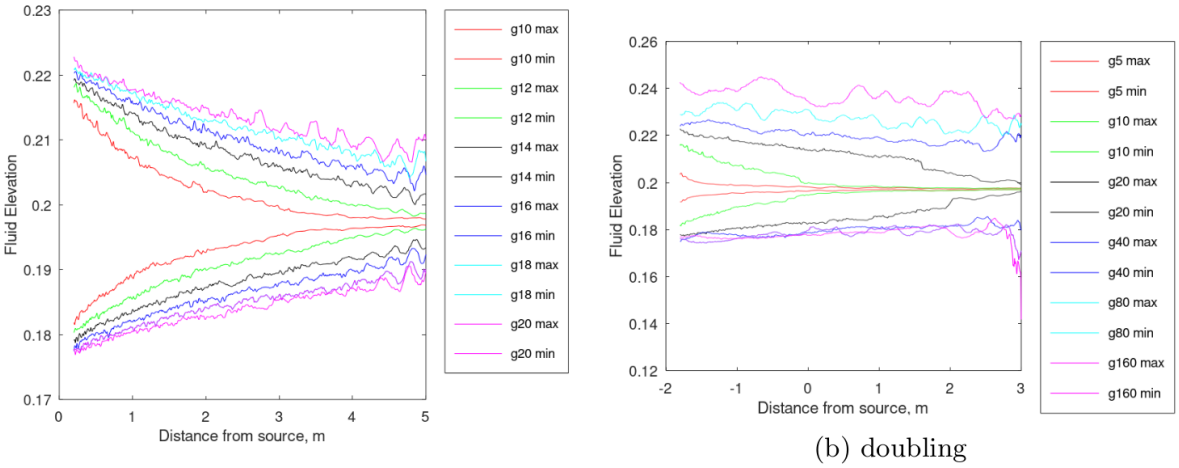

(a) linear increments

(b) doubling

Figure 3. Maximum and minimum water elevation over distance from piston wave source at varying g to visualize rate of surface wave decay for linear increments of gravity strength. Simulated at *simulation default parameters* (see Appendix B) for 10s (a), and 5s (b) physical time.

In examining individual wave forms (specifically, the Fourier transforms) in Figure 4, we also easily see that an increase in wavenumber k as g increases. The discrete Fast-Fourier Transform algorithm (FFT in MATLAB) was used in this case, given generally by (ignoring MATLAB index scheme)

$$fft\big(h(x)\big) \coloneqq H(k) = \sum_{n=0}^{N} h(n) w_N^{kn}, \tag{4}$$

where w_N is given by

$$w_N = e^{j2n/N}. \tag{5}$$

Figure 4 shows the two-sided spectrum from g = 5 to g = 160, thus the closing distance between the two symmetric "spikes" indicated the decrease in wavenumber k with g. In this configuration, increase in gravity roughly corresponds to an even up-scaling in the wave produced, a probable explanation for the increase in longevity.

If the piston is then replaced with the cone (Figure 2), a flavor more loyal to the aim of the paper, running the same simulation now yields a decrease in initial amplitude as g increases. Additionally, at higher gs (g = 30 +), a cone-shaped wave generator will transition to produce waves in distinct groups of two at the

relevant frequency and amplitudes – one wave from the up-stroke and a second from the down-stroke. Despite these differences, the longevity correlation appears to be unchanged, as shown in Figure 5. Figure 5 also appears to indicate a difference in the group velocity of generated waves, as shown by relatively steep drop-offs of fluid elevation at different distances from the wave source, distances at which the surface waves have yet to reach in the time over which the maximum elevation was taken. The group velocity, due to even spacing between the drop-offs, seems to increase linearly with gravity. This is consistent with the understanding of dispersion (waves of longer wavelengths travel faster).

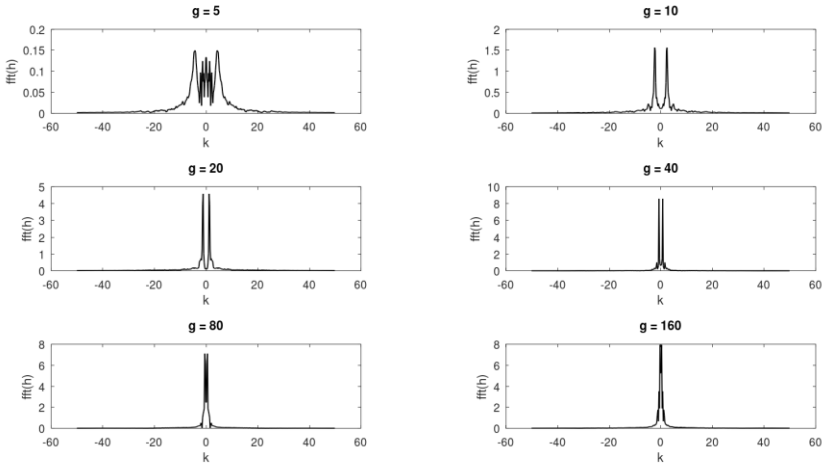

Figure 4. Two-sided wave spectrum of waveform snapshots from g = 5 to 160. Due to resolution limitations using the FFT algorithm, magnitudes shift around drastically and unhelpfully. Spike locations, however are accurate enough to indicate a relationship between and g.

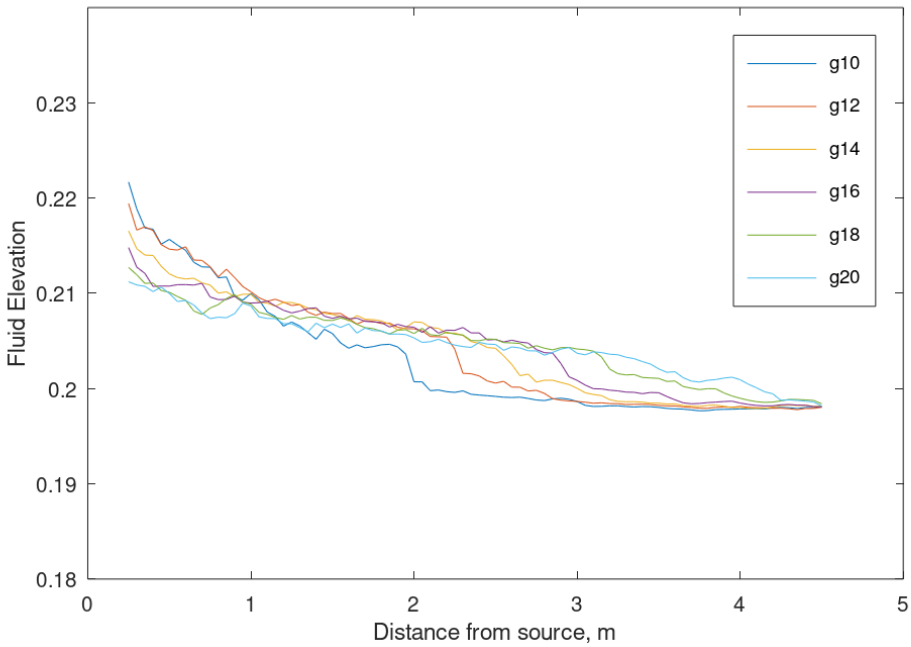

Figure 5. Maximum fluid elevation over distance from wave source for g from 10 to 20. Sharp drop-offs in elevation indicates time-limited wave travel distances.

2.1.2. Wave Absorption

To minimize the reflection of waves off of fixed boundaries, passive wave absorption at outer boundaries was used. Passive wave absorption within DualSPHysics was highlighted in Altomare *et al*. (2017). To put simply, the form of passive wave absorption employed in this paper are impermeable slopes lining the outer edges of the domain. The elliptical domain used for this is shown in Figure 6.

Figure 7 is a test for the absorptive properties of the elliptical boundary in Figure 6, resulting in mainly small and mostly local effects of wave reflection off the boundary.

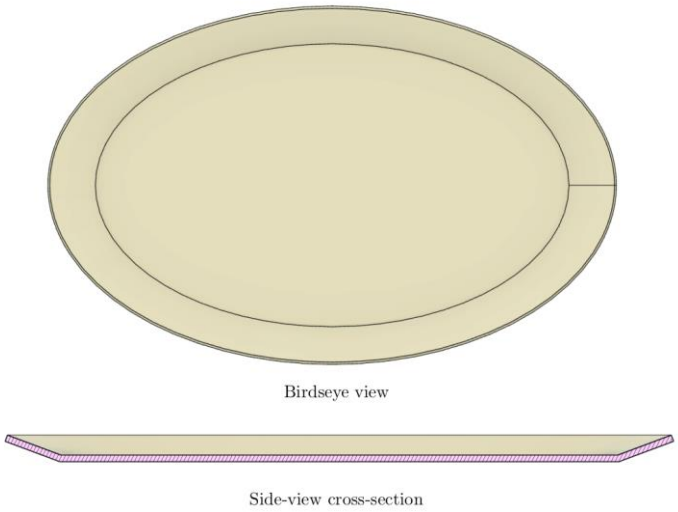

Figure 4. General form of elliptical loft fluid boundary. Examples may use different versions of the general form. Varying dimensions include height, length, width, and taper angle.

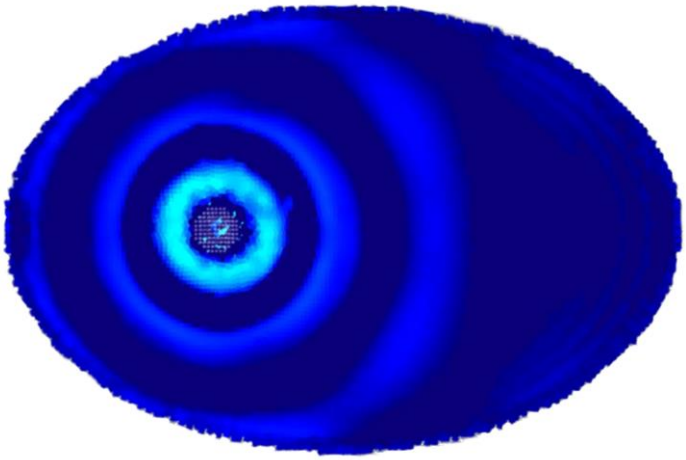

Figure 5. Top view of a test performed on the elliptical wave absorbent boundary container. The wavemaker used in this case is the cone wavemaker with its standard wavemaker parameters (Appendix A.1).

2.2. Wave Interference and Diffraction

At this point, we combine what we have learned so far to construct and optimize cases examining interference and diffraction of surface waves. The goal of the next two studies is to seek out parameters for the clearest illustration of their respective features, them being wave interference and diffraction.

2.2.1. Multiple-Source Interference

The most trivial method to induce interference is to use multiple wave-sources, and of course the simplest case is two identical wave sources displaced from each other an arbitrary amount. Such is the case in our first example. Figure 8 is the resulting interference pattern from two-point wave sources (Figure 2), whose motion was modeled by sinusoidal rectilinear governed by parameters found in Appendix A.2. Figure 9 shows a simulation frame with circular overlays of visually matched radii to predict patches of distinct interference pattern. From the Figures we observe that as the surface waves propagate further from its wavemaker of origin, the location of the peaks and valley diverge from the circular overlays, suggesting an increase in wavelength as the waves propagate, also leading to enlarged "patches" of interference further from the wave sources.

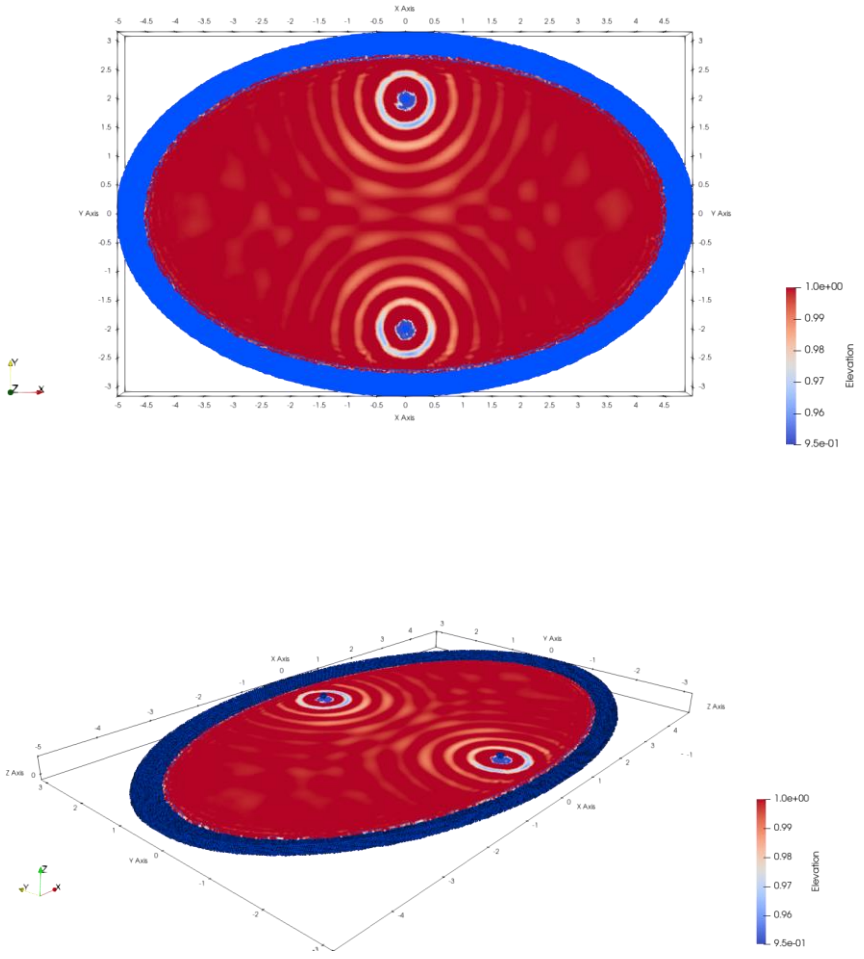

Figure 6. Single simulation frame at the 500th time step showing interference between two wave sources, visualized in *Paraview*.

One aspect requiring attentiveness is the scale relative to the simulated wavelength. It is important to determine the optimal distance between wave sources with respect to wavelength: different distances with respect to the wavelength will yield very different interference patterns, as illustrated by Figure 10. It is also at this point where one may tinker with the general setup to obtain different interference patterns, such as shifting the phase of one wavemaker.

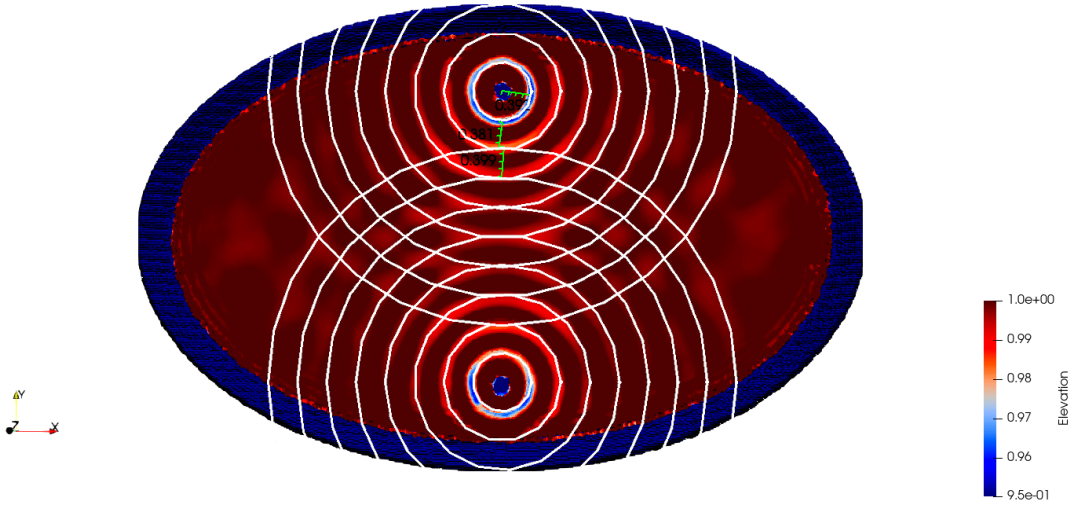

Figure 7. Simulation frame visualized in *Paraview* with circular overlay.

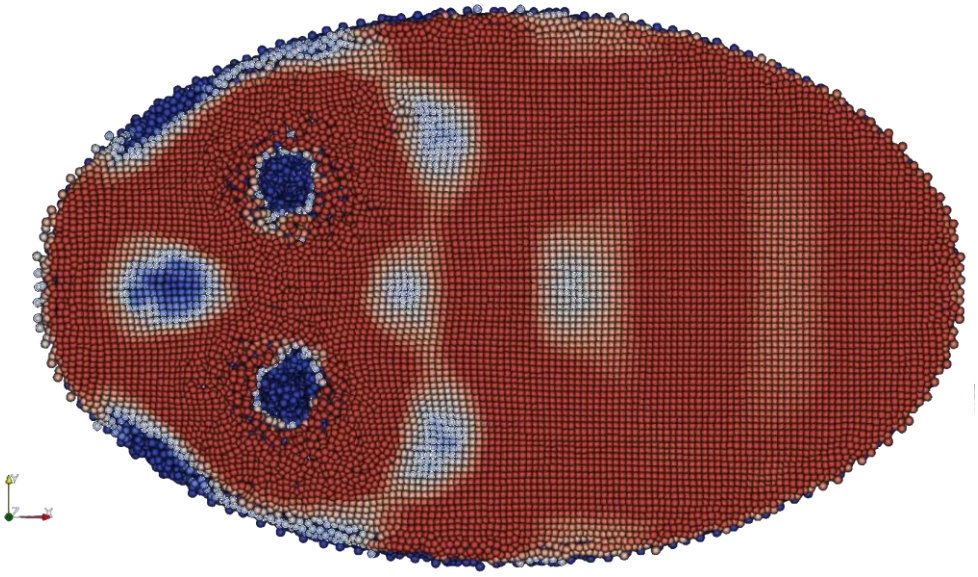

Figure 8. Interference effect at a much smaller scale with respect to interparticle distance and shorter distance between the wavemakers.

In conclusion, this section demonstrates the plausibility of simulating the interference effect from multiple wave sources to a convincing level of realism. It also reveals the importance of and dependency on setup parameters and scale. The importance of scale will become more apparent in the next section.

2.2.2. Diffraction and Double Slit

The next natural step from simple interference is to begin the study of cases in which diffraction from “slits” create "multiple wave sources" from a single wavemaker. The simplest and most well-known example is the double-slit interference - perhaps best known for its feature in the double slit experiment which became the go-to demonstration for the wave-nature of particles in quantum theory. We know the expected outcome of such a case, involving two slits, would be the identical or similar to two individual wavemakers.

In the same exact scale as in Figure 8, we may produce Figure 11. Immediately, we see consequences from inadequacies in design. Despite the extension of wave lifetime from setting a higher value of g = 20, the wave intensity still steadily decreases at a non-negligible rate. The result is that waves will not be discernible without constructive interference. The effects of the decay are amplified by diffraction through the slits, after which the waves intensity is no longer large enough to visualize interference. This forces an increase in sensitivity in color-coding elevation, which gives no extra information and amplifies the noise as well as signal. The resulting Figure 11 is barely able to exhibit the interference between transmitted waves. It is, on the other hand, amusing to point out the much more perceivable interference between reflected and incident waves.

Another challenge is imposed by the design of the barrier on which the two slits reside. In the ideal case, the barrier absorbs all waves with zero reflection. In our configuration, however, the barrier is bound, no different from the boundaries of the fluid container. Such an implementation of a vertical barrier is especially vulnerable to wave reflection, which also contributes to practical noise and the deformation of incident waves. This is considered to be a serious limitation, which could be alleviated by using open-boundary conditions in the future, such as in Verbrugghe et al. (2019).

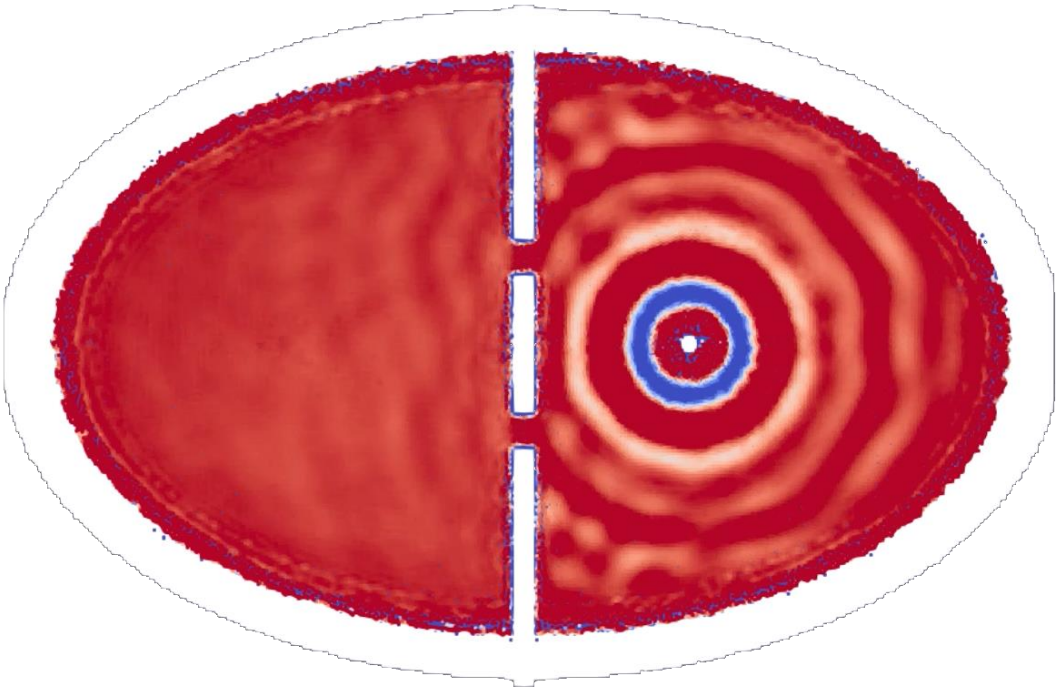

Figure 9. Single simulation frame capturing diffraction (as well as a considerable amount of noise) from two slits in a barrier, using the same scale, resolution, and parameters as in Figure 8.

A phenomenon of interest is observed in the simulation above: In Figure 12, fast waves of an estimated wavenumber 7.5 $m^{-1}$are observed on several timesteps. These waves visually propagate on occasions at surprisingly fast rates, away from point sources along the dividing barrier. Keep in mind, these fast waves were spotted in the *Paraview* visualization. Thus, it is necessary to numerically analyze the data to fully appreciate or dismiss this strange phenomenon.

The cases featured in this section so far and the previous section were able to exhibit wave interference diffraction individually, yet did not satisfactorily produce both simultaneously. To mitigate this limitation, we may turn to simulations in smaller domains, and thus smaller scales. Figure 12 shows the double slit case constructed at the same scale and domain as in Figure 10 of the previous section. In this scale, the deformation of the incident waves is still significant as expected, but the intensity of noise is substantially lower, allowing for the visualization of the interference effect post-diffraction, which seems to follow expectation. In other words, the double-slit case at such a scale is able to demonstrate diffractive-interference akin to two sperate wave sources, albeit at a lower wave intensity.

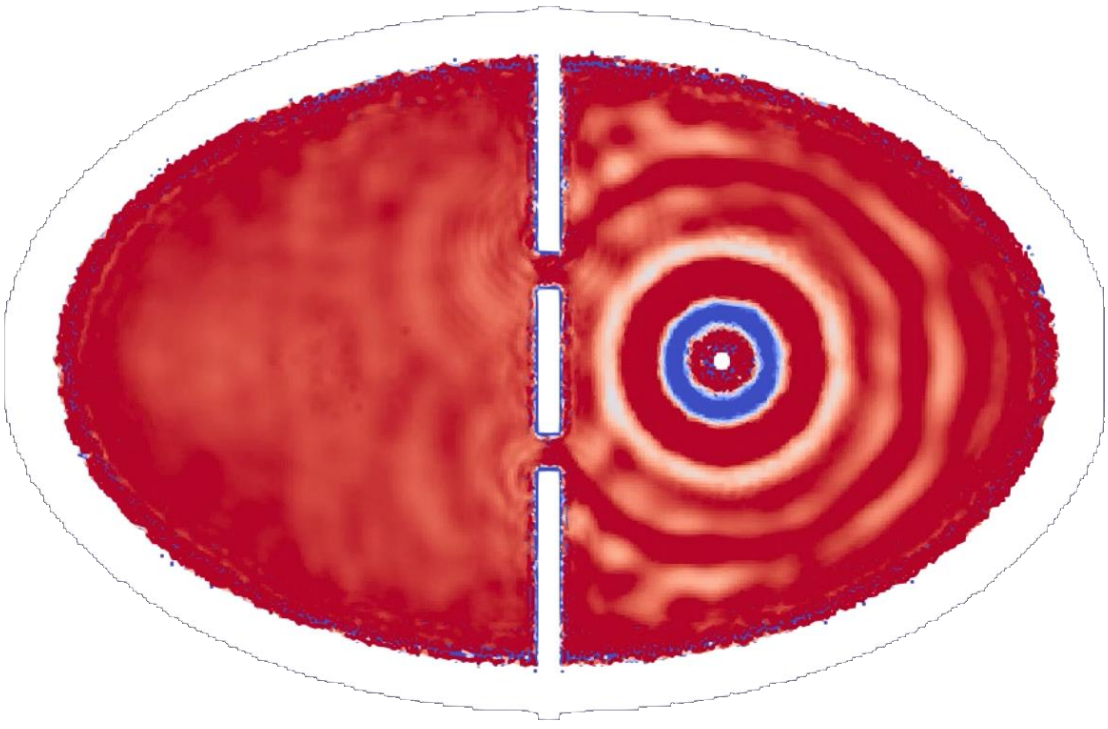

Figure 12. An instance of fast waves phenomenon observed near the barrier.

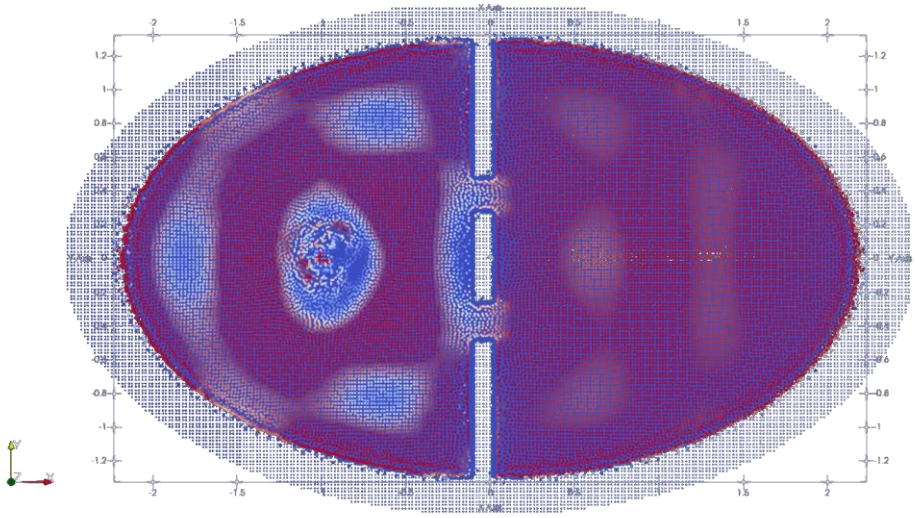

Figure 13. A Double-slit case at the same scale as Figure 8. While it still succumbs to wave deformation, it more clearly exhibits the interference pattern post-diffraction.

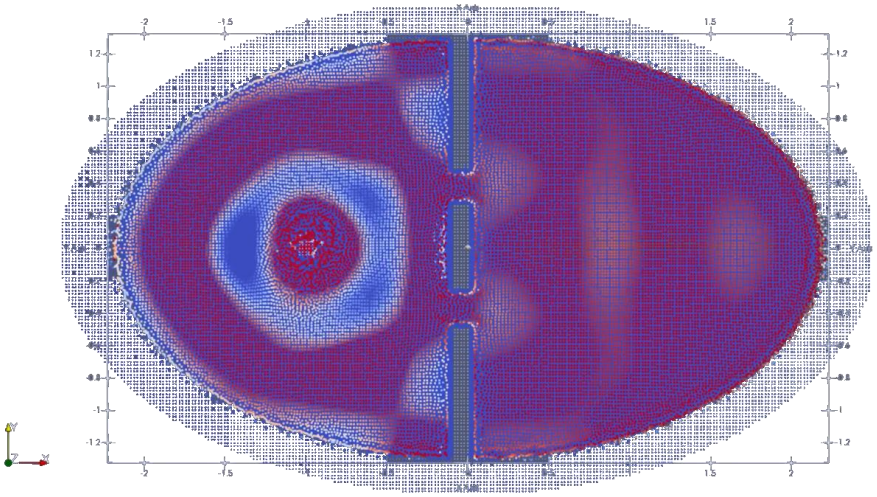

Figure 14. Another frame of the simulation in Figure 13. It shows the wave diffraction through the slits with better clarity than Figure 13.

Before moving on to the discussions, let us conclude this section with some simulation's still frames of the double slit case in the different stages of this project. These frames, despite not fitting into the main body of the paper, still display valuable information about the stages of development, namely, the difficulties faced.

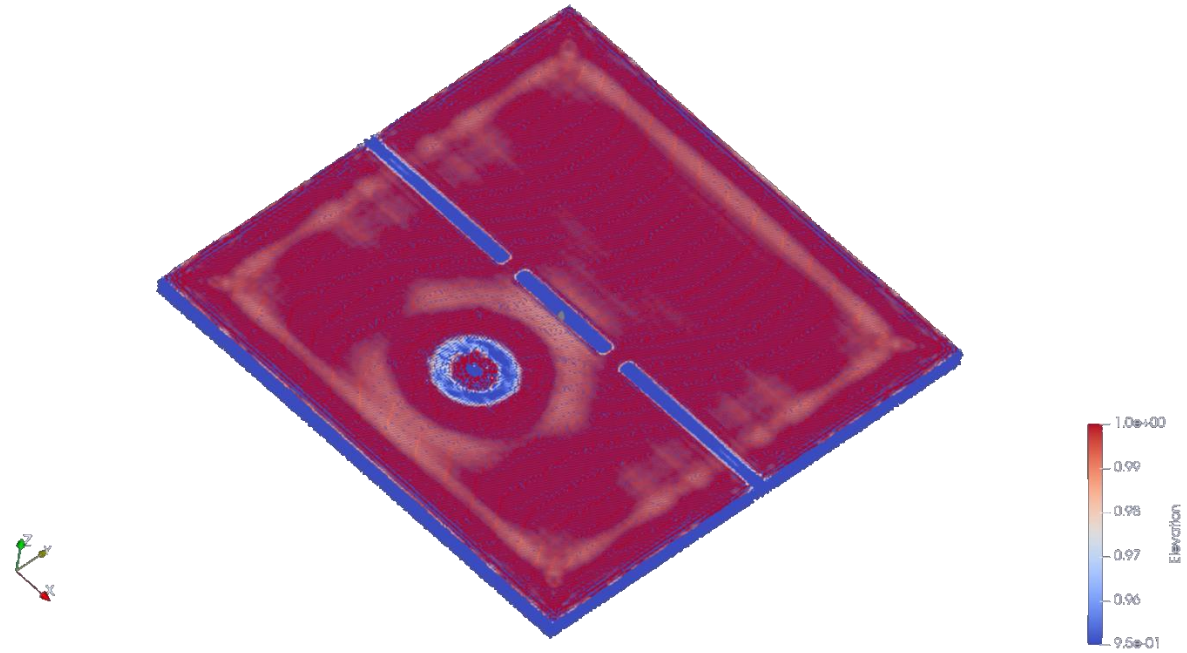

Figure 15. A frame taken from a simulation of a case constructed before the employment of the elliptical boundary. At the boundary, even before reflection could occur, displaced fluid particles form contour waves propagating inwards.

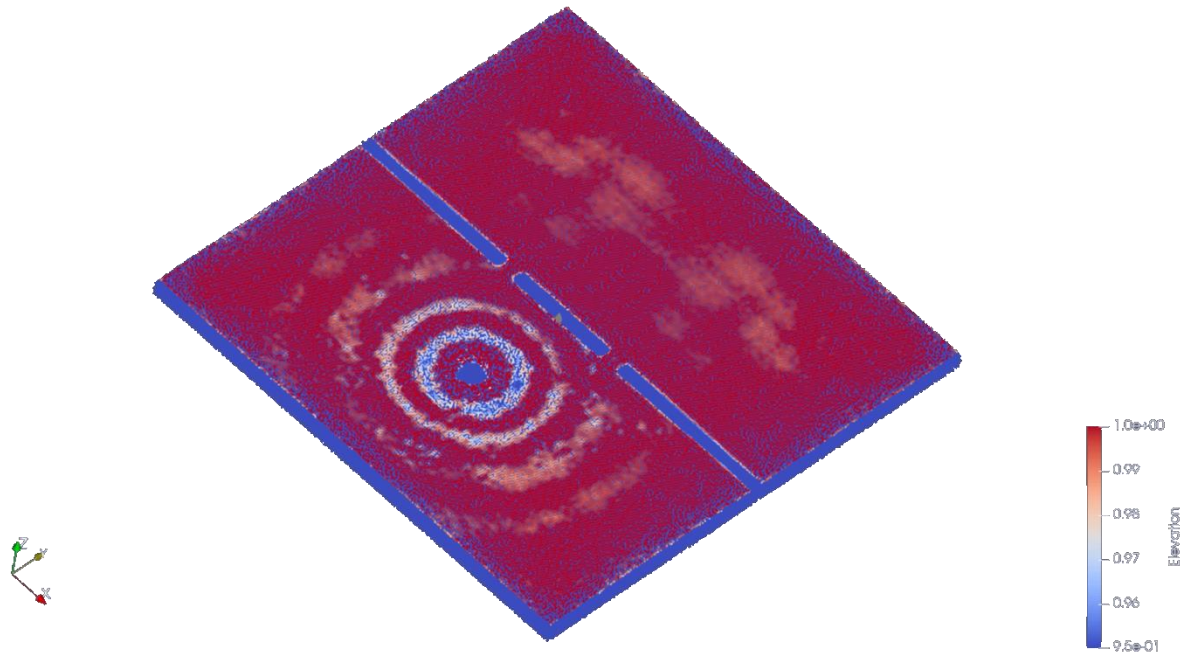

Figure 16. A frame at a later time step shows the deformation to transmitted waves and the interference pattern due to the contour waves in Figure 15.

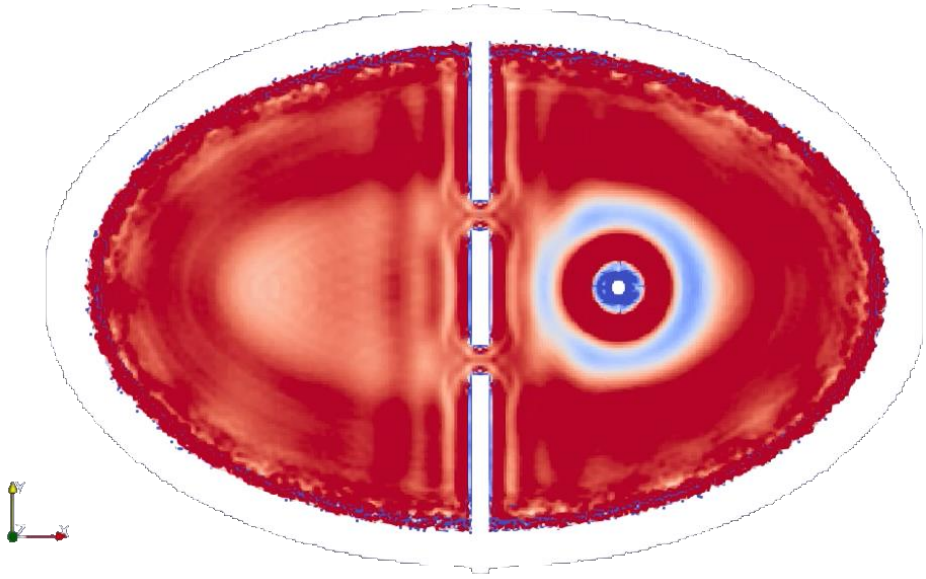

Figure 17. An earlier frame from the simulation in Figure 11. Even the boundary contour waves have been dramatically reduced near the domain boundaries, they still appear due to the vertical dividing

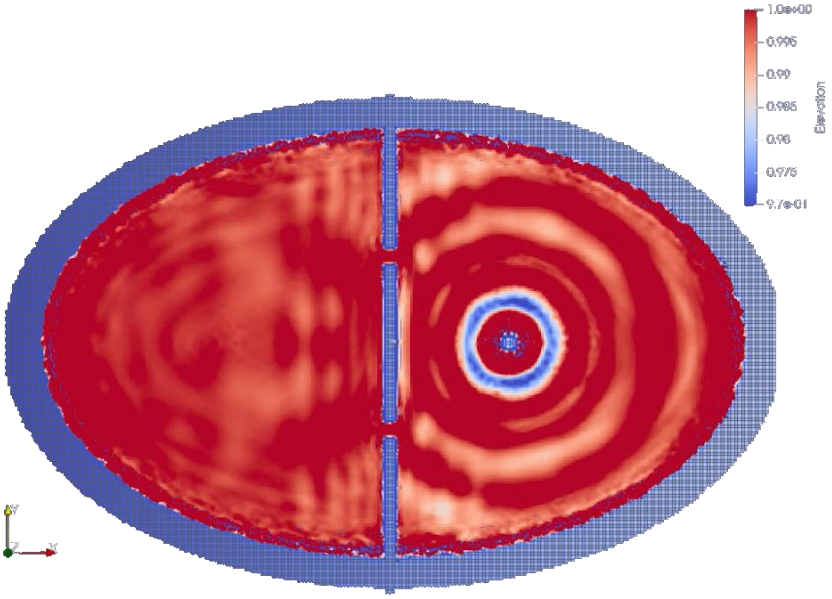

Figure 18. A frame of a separate simulation run of the case in Figure 17 showing the effects of the contour waves on the diffraction and interference patterns.

3. Discussion and Synthesis

The simulations demonstrate the plausibility of applying the SPH computational particle mechanics model for cases involving wave interference and diffraction, but it also reveals the necessity of optimization in simulation configuration and further removal of the model from its intended purpose for more complicated cases, possibly involving finite lattice structures and quasicrystals. The modifications to the model or the constructed cases should in the least include open boundary conditions in various bound features waves are expected to interact with.

3.1 The Consistency of Wave-Gravity Relationship

A curiosity we may have about the above results is the realism the model's relationship between g and various wave properties: amplitude, wave number, and lifetime. We contend that the increased wave longevity with gravity is due to the increase in wavelength, accompanied by an increased group speed (phase speed, in our case, should be identical to group speed). We may attempt to apply airy wave theory (with the pre-requisite that height/wavelength and height/wave height are small), which implies linearity and should give a reasonable approximation away from the container boundaries (where wave linearity breaks).

According to airy wave theory, the mean energy of a fluid surface wave is given by (Andersen & Frigaard, 2011)

$$E = E_k + E_p = \frac{1}{8}\rho H^2, \tag{6}$$

where E is the mean total energy, E_k and E_p are mean kinetic and mean potential energy respectively, ρ is the fluid density, and H is the fluid elevation. The dispersion relation is given by

$$\omega^2 = gktanhkh \tag{7}$$

which can be expressed in terms of phase velocity c:

$$c = \sqrt{\frac{gL}{2\pi}tanh\frac{2\pi h}{L}}, \tag{8}$$

where ω is the angular frequency, $g$is the acceleration due to gravity, k is the wavenumber, c is the phase velocity, and L is the wavelength.

Essentially, for a fluid surface wave with a fixed energy E and angular velocity ω (which should be coupled to the wavemaker),

$$H \propto \frac{1}{\sqrt{g}}, \tag{9}$$

$$c \propto \sqrt{g}. \tag{10}$$

Thus, according to airy wave theory, as gravity strength increases, the wave amplitude should decrease, and the phase speed should increase. This is not consistent with the case using the piston wavemaker (Figure 3) but is somewhat consistent with the case applying the cone wavemaker (Figure 5: longer wavelength and faster group speed). Although it is important to point out that the application of airy wave theory to waves under varying generation conditions inherently flawed (also pointed out by the fact that the limited observed correlation between these quantities is more accurately described as linear, not radical), and further analysis of the wave generation process with various wavemakers is necessary to understand the correlation.

3.2 Limitations in Design

There are several shortcomings to the current design which inhibited the satisfactory fulfillment of the research's goals.

First, as mentioned earlier, the boundary design lacks open boundary conditions, resulting in parasitic wave reflection and deformation of incident and passing waves from bound surfaces. These are especially evident in Figure 14-17. Parasitic wave reflection is most prevalent near completely vertical boundaries, such as the barrier used in the double slit cases. To mitigate this issue completely, it is recommended to replace all current closed boundary surfaces with open bounds moving forward.

Second, the general resolution of the simulations is low. Due to time and hardware equipment limitations, the study fails to explore simulations at higher particle counts, which may yield superior results with regards to noise reduction, smaller features, and visualization. If this contention is valid, it would mean the results obtained from the study cannot be generalized to all SPHysics cases.

3.3 Limitations in Analysis

Mainly due to time constraints, the analysis stage of the study fails to consider several aspects or relationships during the analysis process.

One limitation was of the parameters analyzed during the wavemaker optimization phase. In the study of wave optimization, we only considered g as a potential factor to increase wave longevity, although others may exist. Parameters which were not considered within the analysis includes the viscosity of the fluid, initial interparticle distance, and much more.

The analysis of g's effects on surface waves also demands further investigation. According to 3.1, a constructive relation between wave phase speed and gravity is consistent with the dispersion relation in airy wave theory, this was roughly hinted in Figure 5, which demonstrates an increase in group speed with g. However, in order for such a contention to be fully validated, more analysis in other cases such as the moving boundary piston wavemaker, or similar cases with different wavemaker parameters is required.

Less analysis in general was done for later cases of interference plus diffraction compared to the earlier sections. For instance, the presence of minor features such as fast waves originating along the barrier were not further investigated. A more comprehensive analysis in the future should warrant the use the Fourier transform as well as other analytical tools to determine the presence of these unexplained phenomena.

Appendix A

The following are motion parameters for the moving boundary piston wavemaker and the cone wavemaker respectively. These parameters remain unchanged unless explicitly stated.

A.1 Piston Wavemaker

Raw .xml formatted parameter for the moving boundary pf analytical tools such as the piston wavemaker are provided below.

```
<wavepaddles>
  <piston>
    <mkbound value="1" comment="Mk-Bound of selected particles" />
    <start value="0" comment="Start time (default=0)" />
    <duration value="10.0" comment="Movement duration, Zero is the end of simulation (default=0)" />
    <depth value="0.2" comment="Water depth (default=0)" />
    <pistondir x="1.0" y="0.0" z="0.0" comment="Movement direction (default=(1,0,0))" />
    <waveorder value="2" comment="Order wave generation 1:1st order, 2:2nd order (default=1)" />
    <waveheight value="0.05" comment="Wave height" />
    <waveperiod value="0.5" comment="Wave period" />
    <gainstroke value="1.0" comment="Gain factor to amplify/reduce the paddle stroke (default=1)" />
    <phase value="0.0" comment="Initial wave phase in function of PI (default=0)" />
    <ramp value="0.0" comment="Periods of ramp (default=0)" />
    <savemotion periods="24" period steps="20" xpos="2.0" zpos="-0.15" comment="Saves motion data. xpos and zpos are optional. zpos=-depth of the measuring point" />
  </piston>
</wavepaddles>
```

A.2 Cone Wavemaker

The sinusoidal rectilinear motion preset was used for the cone wavemaker shown below in raw .xml formatting:

```
<freq x="0.0" y="0.0" z="2.0" units_comment="1/s" />
<ampl x="0.0" y="0.0" z="0.05" units_comment="metres (m)" />
<phase x="0.0" y="0.0" z="0.0" units_comment="degrees" />
```

Appendix B

The following are the *default simulation parameters* and constants in .xml formatting. These remain unchanged unless explicitly stated from example to example.

```
<constantsdef>
    <lattice bound="1" fluid="1" />
    <gravity x="0" y="0" z="-9.81" comment="Gravitational acceleration" units_comment="m/s^2" />
    <rhop0 value="1000" comment="Reference density of the fluid" units_comment="kg/m^3" />
    <hswl value="0" auto="true" comment="Maximum still water level to calculate speedofsound using coefsound" units_comment="metres (m)" />
    <gamma value="7" comment="Polytropic constant for water used in the state equation" />
    <speedsystem value="0" auto="true" comment="Maximum system speed (by default the dam-break propagation is used)" />
    <coefsound value="20" comment="Coefficient to multiply speedsystem" />
    <speedsound value="0" auto="true" comment="Speed of sound to use in the simulation (by default speedofsound=coefsound*speedsystem)" />
    <coefh value="1.2" comment="Coefficient to calculate the smoothing length (h=coefh*sqrt(3*dp^2) in 3D)" />
    <cflnumber value="0.2" comment="Coefficient to multiply dt" />
    <h value="0" auto="true" units_comment="metres (m)" />
    <b value="0" auto="true" units_comment="Pascal (Pa)" />
    <massbound value="0" auto="true" units_comment="kg" />
    <massfluid value="0" auto="true" units_comment="kg" />
</constantsdef>
```

```
<parameters>
    <parameter key="SavePosDouble" value="0" comment="Saves particle position using double precision (default=0)" />
    <parameter key="Boundary" value="1" comment="Boundary method 1:DBC, 2:mDBC (default=1)" />
    <parameter key="StepAlgorithm" value="2" comment="Step Algorithm 1:Verlet, 2:Symplectic (default=1)" />
    <parameter key="VerletSteps" value="40" comment="Verlet only: Number of steps to apply Euler timestepping (default=40)" />
    <parameter key="Kernel" value="2" comment="Interaction Kernel 1:Cubic Spline, 2:Wendland (default=2)" />
```

<parameter key="ViscoTreatment" value="1" comment="Viscosity formulation 1:Artificial, 2:Laminar+SPS (default=1)" />

<parameter key="Visco" value="0.01" comment="Viscosity value" /> % Note alpha can depend on the resolution. A value of 0.01 is recommended for near irrotational flows.

<parameter key="ViscoBoundFactor" value="1" comment="Multiply viscosity value with boundary (default=1)" />

<parameter key="DensityDT" value="0" comment="Density Diffusion Term 0:None, 1:Molteni, 2:Fourtakas, 3:Fourtakas(full) (default=0)" />

<parameter key="DensityDTvalue" value="0.1" comment="DDT value (default=0.1)" />

<parameter key="Shifting" value="0" comment="Shifting mode 0:None, 1:Ignore bound, 2:Ignore fixed, 3:Full (default=0)" />

<parameter key="ShiftCoef" value="-2.0" comment="Coefficient for shifting computation (default=-2)" />

<parameter key="ShiftTFS" value="0.0" comment="Threshold to detect free surface. Typically 1.5 for 2D and 2.75 for 3D (default=0)" />

<parameter key="RigidAlgorithm" value="1" comment="Rigid Algorithm 1:SPH, 2:DEM, 3:CHRONO (default=1)" />

<parameter key="FtPause" value="0.0" comment="Time to freeze the floatings at simulation start (warmup) (default=0)" units_comment="seconds" />

<parameter key="CoefDtMin" value="0.05" comment="Coefficient to calculate minimum time step dtmin=coefdtmin*h/speedsound (default=0.05)" />

<parameter key="#DtIni" value="0.0001" comment="Initial time step (default=h/speedsound)" units_comment="seconds" />

<parameter key="#DtMin" value="1e-05" comment="Minimum time step (default=coefdtmin*h/speedsound)" units_comment="seconds" />

<parameter key="DtAllParticles" value="0" comment="Velocity of particles used to calculate DT. 1:All, 0:Only fluid/floating (default=0)" />

<parameter key="TimeMax" value="3.0" comment="Time of simulation" units_comment="seconds" />

<parameter key="TimeOut" value="0.01" comment="Time out data" units_comment="seconds" />

<parameter key="PartsOutMax" value="1.0" comment="%/100 of fluid particles allowed to be excluded from domain (default=1)" units_comment="decimal" />

<parameter key="RhopOutMin" value="700" comment="Minimum rhop valid (default=700)" units_comment="kg/m^3" />

<parameter key="RhopOutMax" value="1300" comment="Maximum rhop valid (default=1300)" units_comment="kg/m^3" />

```
<simulationdomain comment="Defines domain of simulation (default=Uses minimum and maximum position of the generated particles)" >
    <posmin x="default" y="default" z="default" comment="e.g.: x=0.5, y=default-1, z=default-10%" />
    <posmax x="default" y="default" z="1"/>
  </simulationdomain>
</parameters>
```

References:

Altomare, C., Domínguez, J. M., Crespo, González-Cao, Suzuki, Gómez-Gesteira, & Troch. (2017). Long-crested wave generation and absorption for SPH-based DualSPHysics model. *Coastal Engineering*, 37–54.

Andersen, T. L., & Frigaard, P. (2011). *Lecture Notes for the Course in Water Wave Mechanics.* Aalborg: Department of Civil Engineering, Aalborg University.

Domínguez, J. M., Foutakas, G., Altomare, C., R.B., C., Tafuni, A., García-Feal, . . . Gómez-Gesteira. (2021). DualSPHysics: from fluid dynamics to multiphysics problems. *Computational Particle Mechanics*.

Draycott, S., Li, Y., Stansby, P., Adock, T., & van den Bremer, T. (2022). Harmonic-induced wave breaking due to abrupt depth transitions: An experimental and numerical study. *Coastal Engineering*, 104041.

Hughes, S. A. (1993). *Physical Models and Laboratory Techniques in Coastal Engineering* (Vol. 7). WORLD SCIENTIFIC.

Lowe, R. J., Altomare, C., M.L., B., da Silva, R. F., Hansen, J. M., & Crespo, A. J. (2022). Smoothed Particle Hydrodynamics simulations of reef surf zone processes driven by plunging irregular waves. *Ocean Modelling*, 101945.

Verbrugghe, T., Domínguez, Altomare, Tafuni, Vacondio, Troch, & Kortenhaus. (2019). Non-linear wave generation and absorption using open boundaries within DualSPHysics. *Computer Physics Communications*, 46–59.

Violeau, D., & Rogers, B. (2016). Smoothed particle hydrodynamics (SPH) for free-surface flows: past, present and future. *Journal of Hydraulic Research*, 1-26.